SF2A 2011
G. Alecian, K. Belkacem, R. Samadi and D. Valls-Gabaud (eds)

SCATTERING POLARIZATION OF MOLECULAR LINES AT THE SOLAR LIMB

I. Milić[1] and M. Faurobert[2]

Abstract. Molecular lines formed in the upper photosphere of the Sun show linear scattering polarization, when one observes close to the solar limb. This provides us with a diagnostic tool for measuring weak magnetic fields in the solar photosphere through the differential Hanle effect in these lines. However, in order to interpret polarization ratio measured in different lines of different optical thickness, one has to model accurately enough the line formation processes. Observations performed close to and above the solar limb give access to the still poorly known region of the temperature minimum between the photosphere and the chromosphere. The modeling of such observations requires to account for the spherical geometry of the solar atmosphere. Here we revisit the modeling of molecular solar line scattering polarization in spherical geometry and we investigate its diagnostics potential.

Keywords: line: formation, techniques: spectroscopic, Sun: photosphere, Sun: magnetic fields

1 Introduction

The linear polarization of the solar spectrum, observed close to the solar limb, is due to the scattering of the photospheric radiation field in spectral lines, and to Rayleigh and Thomson scattering in the continuum. Line scattering polarization is modified by collisions and by the Hanle effect of weak magnetic fields. Some weak absorption lines, such as the molecular lines of C_2 and MgH, show relatively large linear scattering polarization at the solar limb (Gandorfer 2000). Molecular lines with different sensitivities to magnetic fields may provide us with a model-independent diagnostics of weak magnetic fields, through the differential Hanle effect (Berdyugina & Fluri 2004; Bommier et al. 2006). However, line polarization rates are also affected by depolarizing collisions and radiative transfer, so the interpretation of the differential Hanle effect in lines with different optical depths requires accurate modeling of the line formation process.

Here we investigate the effect of taking into account the spherical geometry of the solar atmosphere. There are several reasons why this should affect the degree of scattering polarization. The most important one being that at the solar limb, the line of sight intersects only a finite part of the solar atmosphere and crosses a more dilute medium, where scattering processes dominate (see Fig. 1). In the following we consider as test cases the MgH line at 515.98 nm and the C_2 line at 515.96 nm and we compare the results for plane-parallel and spherical geometries. We use FALC and FALX solar models (Fontenla et al. 1990) in order to inspect the effects of different temperature distributions on line and continuum polarization. We solve the polarized radiative transfer problem for the lines and continuum background radiation using a two-level formulation of the line source function, without any approximation regarding the optical thickness of the line forming region. Elastic and inelastic collisions play an important role in the scattering mechanism but their rates are presently poorly known for the molecular lines that we are considering. We use estimates derived by Milic & Faurobert (2011) and Bommier et al. (2006) for these quantities. In Sect. 2 we describe the polarized transfer problem and our method for solving it. Results for the linear polarization in spherical geometry are presented in Sect. 3.

[1] Astronomical observatory Belgrade, Volgina 7, 11060 Belgrade, Serbia
[2] UMR 6525 H. Fizeau, Université de Nice Sophia Antipolis, CNRS, Observatoire de la Côte dŠAzur, Campus Valrose, 06108 Nice, France

2 Radiative transfer

2.1 Transfer equation

In the absence of magnetic field (or in the case of a microturbulent, i.e. weak and unresolved, magnetic field), for axially-symmetric radiation field, only two components of the radiation field Stokes vector are different from zero, so we can write $\hat{I} = (I, Q)^\dagger$ and cast the radiative transfer equation along the ray in following form,

$$\frac{d\hat{I}}{d\tau} = (\phi_\nu + \beta)(\hat{I} - \hat{S}), \tag{2.1}$$

where $\hat{S}$ is the source function vector, τ is line-integrated optical depth along the ray, ϕ_ν the absorbtion profile and β the continuum-to-line opacity ratio. The total source function vector can be written as a weighted sum of the line and continuum source functions,

$$\hat{S} = \frac{\phi_\nu \hat{S}_l + \beta \hat{S}_c}{\phi_\nu + \beta}. \tag{2.2}$$

Dealing with weak molecular lines, it is reasonable to assume complete redistribution, we also assume here that the line may be modeled with a two-level formalism, so the line source vector is written,

$$\hat{S}_l(\tau, \mu) = (1 - \epsilon)\frac{1}{2}\int_{-\infty}^{\infty}\int_{-1}^{1} \hat{P}(\mu, \mu')\hat{I}(\tau, \mu', \nu)d\mu' \phi_\nu d\nu + \epsilon B_t(\tau), \tag{2.3}$$

and the continuum source function as,

$$\hat{S}_c(\tau, \mu) = (1 - \epsilon_c)\frac{1}{2}\int_{-1}^{1} \hat{P}(\mu, \mu')\hat{I}(\tau, \mu', \nu)d\mu' + \epsilon_c B_t(\tau), \tag{2.4}$$

where μ and μ' denote respectively the cosines of the heliocentric angles of the outgoing and ingoing radiation propagation direction. The coefficient ϵ is the branching ratio for collisional destruction of line photons. In the continuum source function, $\epsilon_c = \chi_{abs}/(\chi_{sc} + \chi_{abs})$, where χ_{abs} and χ_{sc} denote respectively the absorption and scattering continuum opacities. B_t is the Planck function and $\hat{P}(\mu, \mu')$ is the scattering phase matrix. In the non-magnetic case or in the presence of a microturbulent weak magnetic field, it is given by

$$\hat{P}(\mu, \mu') = \hat{P}_{is} + \frac{3}{8} W_2 W_c W_B \hat{P}_2^0, \tag{2.5}$$

$\hat{P}_{is}$ is the isotropic matrix, and $\hat{P}_2^0$, the anisotropic part of the phase matrix, is given by

$$\hat{P}_2^0 = \begin{pmatrix} (\frac{1}{3} - \mu^2)(1 - 3\mu'^2) & (1 - 3\mu^2)(1 - \mu'^2) \\ (1 - \mu^2)(1 - 3\mu'^2) & 3(1 - \mu^2)(1 - \mu'^2) \end{pmatrix} \tag{2.6}$$

W_2 is the intrinsic polarizability, W_c is the collisional depolarization coefficient and W_B the Hanle depolarization coefficient. Neglecting inelastic collisions, we have

$$W_c = \frac{\Gamma_r}{\Gamma_r + D^{(2)}}, \tag{2.7}$$

where Γ_r is the line radiative damping and $D^{(2)}$ is the depolarizing collision rate. In this study we are mainly interested in the effect of spherical geometry on the modeling of scattering polarization in lines and continua observed at the solar limb, so we set $W_B = 1$.

The continuum radiation is not affected by collisional and Hanle depolarization, the relevant phase matrix is the Rayleigh phase matrix $\hat{P} = \hat{P}_{is} + \frac{3}{8}\hat{P}_2^0$. Here, the absorption and scattering opacity in the continuum are derived from the Uppsala package, using FALC and FALX quiet sun models.

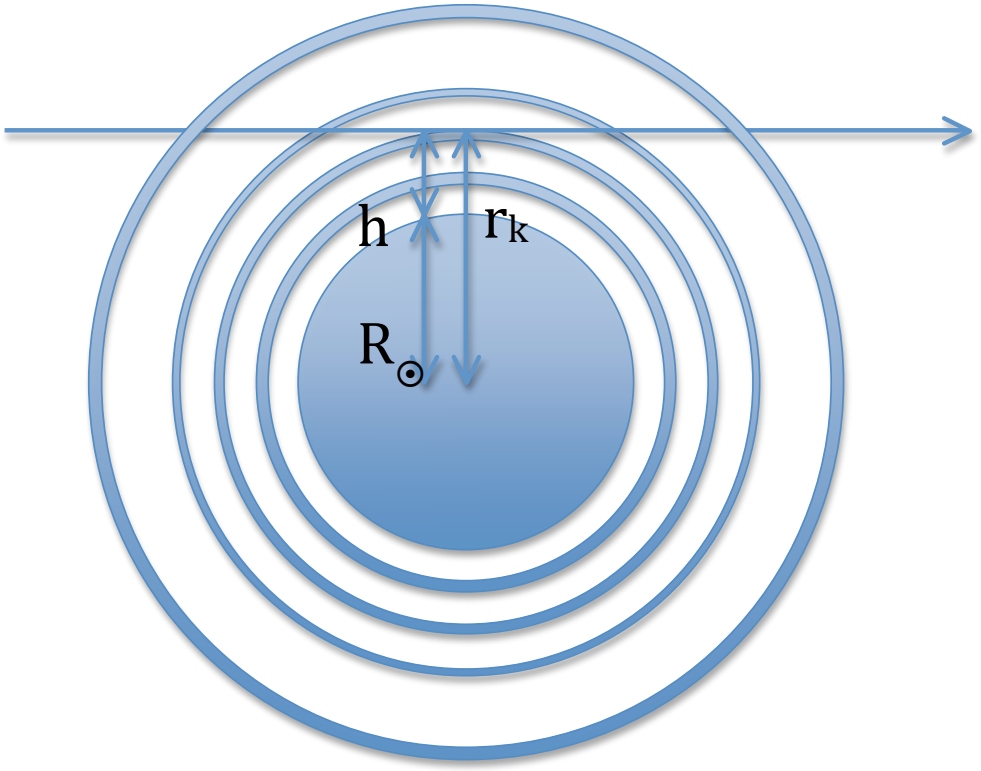

Fig. 1. Geometry of radiative transfer with sphericity taken into account. The line of sight with impact parameter r_k is located at height h above the solar limb, i.e. $r_k = R_\odot + h$.

2.2 Solving the radiative transfer problem in spherical geometry

First, let us notice that, since the solar atmosphere is very thin compared to the solar radius, sphericity effects will be important for very inclined lines of sight only. As they play a negligible role in the angle averaged intensity, level populations and line absorption coefficients may be computed in plane-parallel geometry and the source function for the intensity is weakly affected by sphericity effects. In a first step, we solve the scalar radiative transfer problem for the intensity, neglecting polarization and assuming a plane-parallel geometry. After obtaining self-consistent values for the scalar source function, we take into account polarization and spherical geometry. We start with the assumption $\hat{S} = (S, 0)^\dagger$, where S is the scalar source function computed in the previous step and proceed iteratively, solving in turn the polarized transfer equation and computing the source functions, until convergence. This iterative solution is in essence an ordinary Λ iteration for the polarization, which converges relatively fast, in less than 10 iterations.

When solving the radiative transfer equation in spherical geometry, we avoid the partial differential equation form by using the simpler, "along the ray" approach, as described, for example, by Avrett & Loeser (1984). We compute the scattering integral at each depth point with an angular grid containing both "core-rays" and "surface rays". Core-rays are rays which intersect the solar disk, whereas surface rays go across the limb. The lower boundary condition for core-rays is derived from the diffusion approximation, whereas, for surface-rays, we prescribe a condition of symmetry of the radiation field at the central depth point. In order to get a fine angular mesh at the surface, we use 40 core-rays and as many surface-rays as depth points in the atmospheric model. In the following we consider the line-of-sight limb distance δ, given in arcsec by

$$\delta = \frac{h}{R_\odot} \times 960'', \tag{2.8}$$

where h denotes the altitude of the line of sight with respect to the solar limb. As usual, we define the limb as the point where the continuum limb darkening curve $I(\delta)$ changes its behavior from concave to convex. From our computations we find that the solar limb is located 325 km above the continuum formation height, for both FALC and FALX models. This point is also used to define the solar radius.

2.3 Molecular data

The line integrated opacity, neglecting stimulated emission, is given by

$$\chi = \frac{n_l h\nu}{4\pi} B_{lu}, \tag{2.9}$$

where n_l is the lower level number density and B_{lu} is the Einstein's coefficient of radiative excitation which follows from the coefficient of spontaneous emission A_{ul}.

The MgH line belongs to the Q band of the $A^2\Pi - X^2\Sigma^+(0,0)$ transition, with $J = 16$, J being the rotational lower level quantum number, the C_2 line belongs to the $P3$ band of the $A^3\Pi_g - X^3\Pi_u$ transition with $J = 26$. The molecular number densities obey the equilibrium equation, given by e.g. by Berdyugina et al. (2003):

$$\frac{n(A)n(B)}{n(AB)} = K_{AB}, \tag{2.10}$$

where, $n(AB)$, $n(A)$ and $n(B)$ are, respectively, the molecule number densities and the constituting atom densities, and K_{AB} is the equilibrium constant. In general, equilibrium constants depend on temperature, partition functions of molecule and constituting atoms and on the dissociation energy of the molecule. Convenient polynomial expressions for equilibrium constants and molecule partition functions are given by Sauval & Tatum (1984). In general, in order to obtain exact molecular number densities, one should take into account all molecules and all constituting atoms and solve a system of non-linear equations as explained by Berdyugina et al. (2003). However, due to relatively high temperatures, molecular densities are small, so when computing the MgH density, we may approximate n(Mg) with the total number density of magnesium derived from its abundance relative to hydrogen. The situation is a bit more complicated when it comes to computing the C_2 density, due to the presence of CO whose number density may be a significant fraction of the total number density of carbon, especially in cool regions of the atmosphere. So we consider both CO and C_2 molecules in equilibrium with atomic carbon and oxygen. Then to compute the line opacity, we assume that for weak molecular lines the population of the lower level of the transition follows the LTE law. We adopt the values of A_{ul} given by Faurobert & Arnaud (2003).

In the case of molecular lines, elastic collisions are mainly due to neutral hydrogen atoms and both electrons and neutral hydrogen contribute to inelastic collisions (Shapiro et al. 2011). As accurate collision rates are presently not available for the molecular lines we are considering here, we use the empirical values derived by Milic & Faurobert (2011) and Bommier et al. (2006).

3 Results and discussion

3.1 Optical paths and line optical depth

We find that both molecules are mostly concentrated in a 200 km wide slab located about 100 km above the base of the photosphere, and that the number density of C_2 is a factor of 10 larger than that of MgH. In case of FALC model, the MgH line center optical thickness, measured along the radial direction, is 0.17 at the base of the photosphere, the C_2 line is thicker, its optical thickness along the radial direction is larger by almost a factor of 3 (≈ 0.45). Radial optical depths computed with the FALX model are very similar, except in the region of the temperature minimum around $z = 500$ km, where molecular densities are larger due to cooler temperatures in the FALX model. Let us now see the behavior of the line optical depths measured along the line-of-sight.

The left panel of Fig. 2 shows the variations of the line-of-sight optical depth as a function of limb distance for both the MgH and C_2 lines and the FALC model. We compare the results obtained in plane-parallel and spherical geometries for lines of sight close to the limb. There is little difference between both geometries when the limb-distance is larger than 5 arcsec, but they differ significantly at smaller limb distances. An important thing to keep in mind is that, in spherical geometry, the optical path does not scale with observing direction as simply as $\Delta\tau_{los} = \Delta\tau/\mu$ (see Fig. 2). It shows a sharp maximum, for both lines, at $\delta \simeq -0.3$". This value corresponds to the lines of sight which go through the molecular layer. Moving the line of sight outwards, we mainly observe above the molecular layer, as a consequence the line optical depth rapidly goes to zero. In plane-parallel geometry any line of sight always intersect the molecular layer, and the length of its path increases when we go closer and closer to the limb, so that the line optical depths keep increasing. In plane-parallel geometry we cannot model observations performed outside the limb.

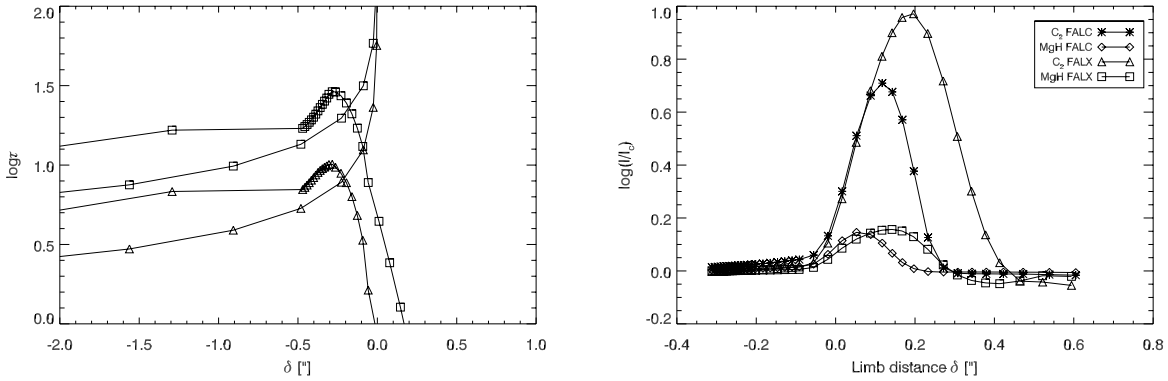

Fig. 2. Left: Comparison of line center optical path for spherical and plane-parallel geometry (triangles for MgH , and squares for C_2). **Right:** Intensity at line center divided by the continuum intensity, in both models as a function of limb distance. When observed above the limb, lines are seen in emission, but quickly disappear.

3.2 Line intensities and scattering polarization.

The right panel of Fig. 2 shows the emergent intensities at line center for the MgH and C_2 lines , for spherical symmetry with FALC and FALX models, as functions of limb distance. Both lines go into emission above the solar limb, for limb distances smaller than 0.4 arcsec, and quickly disappear at larger limb distances. This is consistent with the observations reported by Faurobert & Arnaud (2002). When observed inside the limb both lines are very weak absorption lines. The emission seen above the limb cannot be modeled in plane-parallel geometry.

Figure 3 presents the comparison of the emergent polarization at line centers, as functions of δ, computed in spherical and plane-parallel geometries, with FALC and FALX models. Both geometries give the same results at limb distances larger, in absolute value, than 5", but they differ significantly at smaller limb distances. We notice that the polarization rate shows a maximum, in absolute value, for the lines of sight where the optical path shows a maximum (see Fig. 2). That fact can be qualitatively explained in the following way, as the slab optical thickness increases, the probability that a photon will be scattered in the line increases. So the polarization increases. At larger distance above the limb the line optical depth decreases. This gives rise to the local polarization maximum that we see in Fig. 3. The polarization starts increasing again at larger distance from the limb, where the line has disappeared (see Fig. 2). We then see the continuum polarization only, it increases because continuum scattering opacity increases in the low chromosphere. We notice that with the FALC model, values of the polarization maxima between 2% and 2,5% are consistent with the measurements reported by Faurobert & Arnaud (2002), for the molecular lines seen in emission above the solar limb. With FALX we recover the same general behavior as with the FALC model, but with much larger polarization rates, the maximum reaches values on the order of 10 %. Such large rates have not been observed close to the solar limb.

4 Conclusions

Taking into account the spherical geometry of the solar atmosphere allows us to compute the intensity and scattering polarization of the solar spectrum at the limb. We have found that for our test-case lines of C_2 and MgH, scattering polarization shows maxima of a few percents at about 0.3 arcsec above the limb, where the lines are in emission. The order of magnitude of these polarization maxima are consistent with the observed rates when the FALC quiet sun model is used but the FALX model leads to much larger polarization rates.

The polarization maxima observed at 0.3" above the solar limb correspond to lines of sight crossing the temperature minimum region between the photosphere and the chromosphere. More limb observations are needed to make use of the differential Hanle effect in different molecular lines in order to investigate this region. Such observations require few scattered light in the instrument and good seeing conditions.

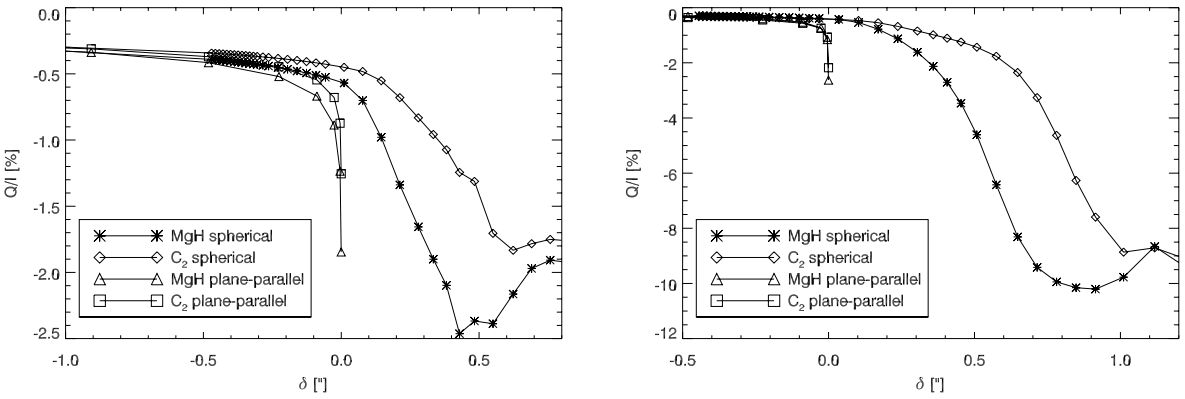

Fig. 3. Linear polarization at line center as a function of limb-distance for the MgH line (asterisks for spherical and triangles for plane-parallel case) and the C_2 line (diamonds for spherical and squares for plane-parallel case). **Left**: FALC model. **Right**: FALX model

References

Avrett, E. H. & Loeser, R. 1984, Line transfer in static and expanding spherical atmospheres, ed. Kalkofen, W., 341–379

Berdyugina, S. V. & Fluri, D. M. 2004, A&A, 417, 775

Berdyugina, S. V., Solanki, S. K., & Frutiger, C. 2003, A&A, 412, 513

Bommier, V., Landi Degl'Innocenti, E., Feautrier, N., & Molodij, G. 2006, A&A, 458, 625

Faurobert, M. & Arnaud, J. 2002, A&A, 382, L17

Faurobert, M. & Arnaud, J. 2003, A&A, 412, 555

Fontenla, J. M., Avrett, E. H., & Loeser, R. 1990, ApJ, 355, 700

Gandorfer, A. 2000, The Second Solar Spectrum: A high spectral resolution polarimetric survey of scattering polarization at the solar limb in graphical representation. Volume I: 4625 Å to 6995 Å, ed. Gandorfer, A.

Milic, I. & Faurobert, M. 2011, A&A, submitted

Sauval, A. J. & Tatum, J. B. 1984, ApJS, 56, 193

Shapiro, A. I., Fluri, D. M., Berdyugina, S. V., Bianda, M., & Ramelli, R. 2011, A&A, 529, A139+